0038-075X/94/1586-0421$03.00/0
SOIL SCIENCE
Copyright © 1994 by Williams & Wilkins

December 1994
Vol. 158, No. 6
Printed in U.S.A.

MAPPING OF SELENIUM CONCENTRATIONS IN SOIL AGGREGATES WITH SYNCHROTRON X-RAY FLUORESCENCE MICROPROBE

TETSU K. TOKUNAGA,[1] STEPHEN R. SUTTON,[2] AND SASA BAJT[2]

The possible occurrence of reducing microsites in synthetic soil aggregates and their influences on the distribution of selenium species with redox-dependent mobilities was tested using the synchrotron X-ray fluorescence microprobe (SXRFM). Synthetic, effectively two-dimensional soil aggregates of diameters ranging from 10 to 30 mm were constructed, with and without inclusion of sections of *Scirpus robustus* and *S. californicus* root sections. Each aggregate was uniformly wetted with a saline solution containing 240 g m^{-3} Se [98% as Se(VI), and 2% as Se(IV)]. Gas-phase porosities varied between individual aggregates from 0.00 to 0.40 and were maintained relatively constant during the incubation period of up to 17 days. Exchanges of soil gases with atmospheric air occurred only along the periphery of the aggregates. Scanning of the aggregates using SXRFM demonstrated that Se was essentially homogeneously distributed in soils without *Scirpus* root sections, suggesting that Se remained primarily as the soluble Se(VI) species. The SXRFM results revealed large accumulations of *total* Se in regions surrounding embedded sections of *Scirpus* roots. As much as 20-fold local enrichment with respect to total Se was measured in water-saturated soils within 1 to 4 mm of decomposing roots. These observations provide support for a model of localized reducing zones in which Se(VI) is reduced to less mobile Se(IV) and to insoluble Se(0), resulting in local accumulation of total Se. The measured Se accumulation in one microsite compared reasonably well with a simple transient Se(VI) diffusion model. It is postulated that such mechanisms may account for similar heterogeneities observable in some Se-contaminated soils at Kesterson Reservoir. Such heterogeneities in concentrations of Se and other constituents within individual soil aggregates have important implications with respect to reactivity and need to be included in any detailed mechanistic modeling of chemical cycling within soils. This work also provides an example of the substantial capabilities of SXRFM in studies of soils.

[1] Earth Sciences Division, Lawrence Berkeley Laboratory, Berkeley, CA 94720.

[2] Department of Geophysical Sciences, and Center for Advanced Radiation Sources, The University of Chicago, Chicago, IL 60637.

Received Jan. 28, 1994; accepted July 6, 1994.

The potential importance of heterogeneous oxygen concentrations within soil aggregates has long been recognized. Within aggregates that physically may be essentially homogeneous, diffusion-limited transport of oxygen, coupled with sufficiently high microbial respiration rates, may promote the generation of internal anaerobic regions. The anaerobic microsite model was developed to explain the observations of denitrification within macroscopically well aerated soil profiles (e.g., Currie 1961; Currie 1965; Smith 1977; Freney et al. 1979; Smith 1980; Leffelaar 1986 and 1993). Although the anaerobic microsite studies cited above provide insight into the coexistence of oxidizing and reducing zones within soil aggregates, their simplicity with respect to uniform distributions of the controlling parameters may be unrealistic in many cases. For example, much higher denitrification rates in the immediate vicinity of particulate organic matter within soil aggregates were measured by Parkin (1987). Regardless of the specific geometry, the coexistence of oxidizing and reducing environments at the aggregate scale (typically in the range of 10 to 10^2 mm in effective diameter) can also have important consequences on the fate of many other elements susceptible to oxidation-reduction reactions in soils.

The importance of understanding redox conditions with respect to the behavior of selenium in soils also has a long history (Anderson et al. 1961; Rosenfeld and Beath 1964; Sharma and Singh 1983). Recently, attention has again been drawn to this problem with Se contamination of Kesterson Reservoir, California, as a result of wildlife deaths and deformities in a wetland supplied with seleniferous agricultural drain

waters (Ohlendorf 1989). Several previous studies have provided information on Se distributions within Kesterson Reservoir soils on the macroscopic scale of individual soil profiles (Weres et al. 1989; Long et al. 1990; Benson et al. 1991; Tokunaga et al. 1991; White et al. 1991; Zawislanski et al. 1992). These macroscopic analyses provide information on Se concentrations and speciation averaged over distances on the order of about 10 to 10^3 mm. A typical distribution of total Se in a Kesterson Reservoir soil profile 4 years after flooding with seleniferous drain waters is shown in Fig. 1. Such profiles exhibited large accumulations of Se within the uppermost regions of ponded sediments, where transformation of ponded Se(VI) to both adsorbable and less soluble reduced species occurred (Weres et al. 1989). In such approaches, the possibility of smaller scale heterogeneities in Se concentrations were not addressed and remain to be determined. The potential significance of such information stems from the need to understand the fate of Se not only in contaminated soils, but in natural soil environments as well. The occurrence of large concentration variations on a smaller scale could imply significantly lower exposed surface areas at which oxidation-reduction, precipitation-dissolution, and adsorption-desorption reactions take place relative to more uniformly distributed concentrations.

The redox- and pH-dependence of Se partitioning between aqueous, solid, and surface phases provides the basis for generating heterogeneous distributions of total Se within systems. When Se is introduced into a system in the soluble Se(VI) state, local enrichment with respect to Se occurs where reducing conditions occur. Under mildly reducing conditions, Se(VI) is transformed to Se(IV) (Elrashidi et al. 1987). Selenite is susceptible to pH-dependent adsorption and/or precipitation (Geering et al. 1968; Neal et al. 1987). Under more strongly reducing conditions, reduction to insoluble Se(0) occurs. Such microbially mediated reduction of Se(VI) operated during deposition of seleniferous drain waters in evaporation ponds at Kesterson Reservoir, resulting in substantially elevated concentrations of total Se within the upper 0.15 m of the soil profiles. Until recently, reduction to Se(0) could only be inferred from indirect evidence obtained through chemical extraction schemes. Recent X-ray absorption spectroscopy studies conducted at the Stanford Synchrotron Radiation Laboratory have provided the first direct evidence for Se(VI) reduction to both Se(IV) and Se(0) in sediments (Pickering et al., 1994).

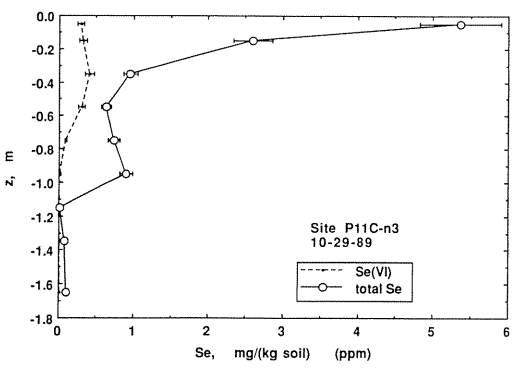

FIG. 1. Profiles of total Se and Se(VI) in a Kesterson Reservoir soil, Pond 11 monitoring site P11C. (Data from Tokunaga et al. 1991).

It appears reasonable that such redox-dependent mobilities could also influence Se redistribution on the considerably smaller scale of individual soil aggregates. When regions with significantly lower redox potentials occur within portions of an aggregate, local reduction of Se(VI) would be expected to promote diffusion of Se(VI) towards the reduced zone from surrounding regions. Such redistribution might also apply for other redox-dependent elements such as Cr, Mn, Fe, Cu, and As, and their microscopic mapping may provide a supplemental approach to investigations of reducing microsite models.

The synchrotron X-ray fluorescence microprobe (SXRFM) provides the capability of mapping elemental distributions at a spatial resolution which, in some cases, approaches ≈ 1 μm, and has several important advantages with respect to studies on soils. The basic principles of the method are analogous to conventional X-ray fluorescence spectroscopy, applied on much smaller target areas. The highly focused, intense X-ray beams needed for such micro-scale analyses are emitted as synchrotron radiation from electrons accelerated around storage rings at facilities such as the National Synchrotron Light Source (NSLS at Brookhaven National Laboratory, Upton, NY) and the Advanced Light Source (at Lawrence Berkeley Laboratory Berkeley, CA). By exposing a sample to such an

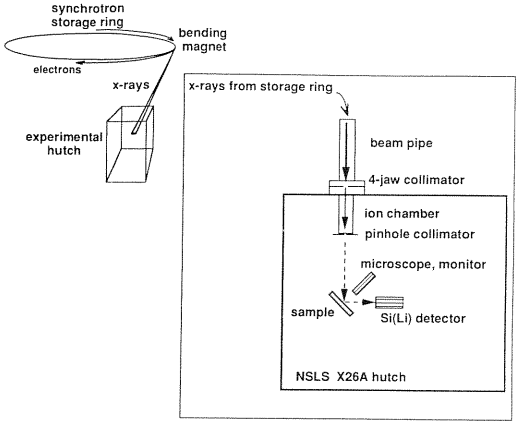

FIG. 2. Basic components of the SXRFM at NSLS (beamline X26A).

intense source of white radiation and measuring the resulting fluorescence spectrum emitted by the specimen, quantification of a range of elements is possible. Scanning a sample through the X-ray beam while simultaneously recording fluorescence spectra provides the opportunity to generate maps of elemental distributions. The basic features of the SXRFM are shown in Fig. 2. Summary articles on the method are found in Jones and Gordon (1989), Wu et al. (1990), Rivers et al. (1991), and Sutton et al., (1993).

In the preliminary portion of this study, the SXRFM was used to map the distribution of Se in soil aggregates collected at Kesterson Reservoir. Results obtained in the preliminary stages of this study motivated the remainder of the laboratory aggregate experiments. These later experiments were designed to test the steady-state anaerobic microsite model as well as a transient Se(VI) diffusion and reduction model as explanations for development of small-scale heterogeneities in total Se concentrations.

THEORY

When the anaerobic microsite model is applied to a spherical aggregate of radius R, characterized by an effective oxygen diffusion coefficient D_{e,O_2}, the critical steady-state respiration rate needed to initiate anaerobiosis is obtainable from O_2 mass-balance considerations. The result,

$$S = \frac{6D_{e,O_2}\, C_{o,O_2}}{R^2}, \qquad (1)$$

where S is the respiration rate and C_{o,O_2} represents the O_2 concentration at the exterior surface of the aggregate follows from Currie (1961). In the case of steady-state radial diffusion in a cylindrical aggregate of radius R, the critical respiration rate is given by

$$S = \frac{4D_{e,O_2}\, C_{o,O_2}}{R^2}. \qquad (2)$$

Equation (2) is derived in the same manner as Eq. (1). The analogous one-dimensional result gives a similar expression with a factor 2 in place of 4. Thus, a general N-dimensional expression, which includes Eqs. (1) and (2) as special cases, contains the factor 2N. The result presented in Eq. (2) will be considered later in the context of radial diffusion of O_2 in synthetic, homogeneous aggregates.

Naturally formed soil aggregates may not exhibit the homogeneous features assumed in the simplest of models. Regions near decomposing plant roots may have higher probabilities of developing anaerobiosis, hence higher probabilities of exhibiting localized accumulations of Se when scanned with the SXRFM. A possible explanation for redox- and diffusion-controlled heterogeneities with respect to total Se concentrations in the vicinity of one particular *Scirpus* root cross-section will be considered in moderate detail. In this case, a root cross-section was embedded with its axis perpendicular to the plane of the two-dimensional soil aggregate. The aggregate was water-saturated with a solution containing Se(VI). If Se(VI) reduction occurs at a specific radial distance in the vicinity of root-soil contact, this zone may be regarded as a cylindrical sink for Se accumulation as indicated in Figure 3a. This figure illustrates the possible diffusion of mobile Se(VI) to the cylindrically-symmetric reducing zone around a decomposing root. The initial condition is represented by a uniform concentration ($C_{o,Se(VI)}$) of Se(VI) in a saturated sediment in two-dimensional space. After ≈1 day, which our past experience indicates represents a typical incubation time needed for reducing conditions to prevail, the reducing region is modeled as a cylindrical surface at which the Se(VI) concentration is zero. Thus, Se(VI) is induced to radially diffuse from the surrounding sediment towards the root zone. This model is mathematically analogous to the radial heat conduction problem solved by Smith (1937) and the problem of groundwater flow to

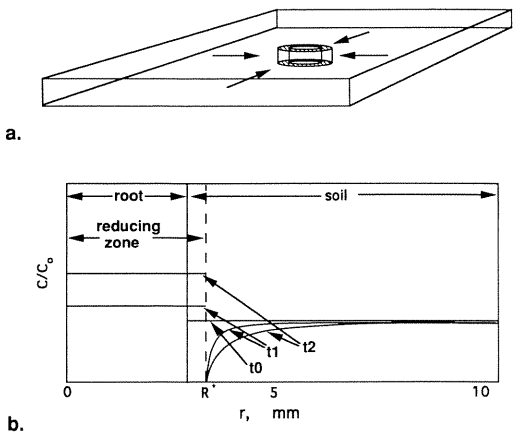

FIG. 3. (a) Representation of a decomposing root cross-section embedded in water-saturated sediment. Both the root-soil interface and a hypothetical surface at which the concentration of Se(VI) becomes 0 due to reduction are shown. (b) Idealized radial distributions for Se(VI) before and after the development of reducing conditions outside the root at R*. The hypothetical Se(VI) distribution is uniform throughout the system at time zero. At later times, the Se(VI) concentrations decrease toward zero as the reducing zone is approached from the soil zone. The Se(IV) and Se(0) hypothetically formed at R* are uniformly distributed within $r \leq R^*$ for purposes of this illustration.

an artesian well analyzed by Jacob and Lohman (1952). Qualitative representations of radial Se distributions at times $t0 < t1 < t2$ are depicted in Figure 3b. In regions outside of the reducing zone, only the hypothetical Se(VI) profiles are shown. The Se(IV) and Se(O) generated by Se(VI) reduction are uniformly distributed within the reducing zone for purposes of this diagram. Following Smith (1937) and Jacob and Lohman (1952), the instantaneous rate at which Se(VI) diffuses into the reducing zone of radius R_e is given (per unit thickness in the axial direction) by

$$Q(t) = [2\pi D_{e,Se(VI)} C_{0,Se(VI)}] G\left(\frac{1}{4u(t)}\right) \quad (3)$$

where $D_{e,Se(VI)}$ is the effective diffusivity of *Se(VI)* in the sediment, the time-dependent parameter $u(t)$ is given by

$$u(t) = \frac{R_e^2}{4D_{e,SE(VI)^t}}, \quad (4)$$

and

$$G\left(\frac{1}{4u(t)}\right) = \frac{1}{\pi u} \int_0^\infty x e^{-x^{2/(4u)}} \left\{\frac{\pi}{2} + \tan^{-1}\left[\frac{Y_0(x)}{J_0(x)}\right]\right\} dx \quad (5)$$

In Eq.[5], x is an integration variable, and Y_0 and J_0 represent Bessel functions of order zero of the first and second kinds, respectively. The effective diffusivity of Se(VI) in water-saturated sediment may be approximated by

$$D_{e,Se(VI)} \approx \alpha f D_{o,SO_4} \quad (6)$$

where f is the (water-saturated) porosity, the complexity parameter α includes porous media influences of tortuosity and mobility (Hillel 1980), and $D_{o,SO_4} \approx 1.1 \times 10^{-3}$ mm^2 s^{-1} is the sulfate diffusivity in water at 27°C (Robinson and Stokes 1959). This latter diffusivity was used because of physical-chemical similarities between sulfate and selenate and because of confidence placed in D_{o,SO_4} values obtained from various independent sources. In addition, estimated values of D_{e,SeO_4} may be compared with reported values of D_{e,SO_4}. We later integrate Eq. (3) to obtain predicted cumulative Se diffused into the reducing zone according to this simple model and compare calculations with measurements obtained with the SXRFM.

MATERIALS AND METHODS

Four natural soil aggregate samples from Kesterson Reservoir were analyzed with the SXRFM. Since the sample preparation and results were similar for each of these, only one aggregate will be described in detail. This field soil aggregate sample was obtained on April 28, 1991, from a depth of about 0.07 m in the former Pond 4 region of Kesterson Reservoir. The soils of this area are mapped as Albic Natraqualfs (Turlock sandy loam, Nazar 1990), although considerable variability of natural and anthropogenic origin is observable within the mapping unit. This site was ponded with seleniferous agricultural drain waters from 1981 to 1986, and primarily vegetated with *Typha latifolia*. The Se concentrations in these saline agricultural drain waters were typically in the range of 250 to 350 mg m^{-3} (250 to 350 ppb). Since 1986, no further disposal of agricultural drain waters occurred at

Kesterson Reservoir, and the Pond 4 sampling site remained covered with a dense surface litter of *Typha* leaves and sparse annual forbs (dominated by *Lactuca serriola*). The ≈5.5-mm-diameter, ≈1.2-mm-thick sample was obtained from a larger (≈8-mm diameter) aggregate. The front (analyzed) surface of the sample was originally a cross-section through the aggregate interior. This surface was obtained by breaking open the original aggregate, without shearing, to expose a fresh surface. The sides and back of natural soil aggregates were trimmed with a razor blade and mounted within a sample-holding cavity on a 50-mm by 50-mm plastic slide frame. The front surface of the sample was flattened by pressing it against the inside of the Mylar film window rather than by slicing in order to avoid smearing of soil particles. This procedure minimized lateral translation of mineral grains to less than 0.3 mm along the newly exposed surface. Such precautions were necessary because the X-ray absorption and fluorescence are heavily weighted to the surface region (<200 μm for Se). The front window, through which synchrotron X-rays entered and fluorescent X-rays exited, consisted of 25-μm-thick Mylar. The absorption of Se fluorescence X-rays by this Mylar film was negligible.

The natural soil aggregate samples were prepared about 3 days before scanning with the SXRFM. Exposure of new surfaces to air during this interval was not expected to significantly alter Se distributions because measured Se reoxidation rates in Kesterson Reservoir soils are relatively slow. For example, data from long-term (1987 to 1992) monitoring of Kesterson Reservoir soils indicates that reoxidation to water-soluble Se(VI) under predominantly vadose conditions occurs at a rate of about 5% of the reduced soil Se pool per year (Tokunaga et al., 1991; and Lawrence Berkeley Laboratory, Earth Sciences Division, unpublished data, 1987–1992). Conversely, rates of Se(VI) reduction in flooded surface soils are typically quite rapid (about 1 to 2 days, from Tokunaga 1987, unpublished data).

The major portion of this study involves a set of laboratory-prepared soil aggregates in which Se was initially homogeneously distributed in the soluble Se(VI) state. The aggregates were constructed to provide a range of conditions with respect to aeration. Six of the disc-shaped aggregates were each effectively homogeneous, with exposure to atmospheric oxygen permitted only along the radial boundaries (i.e., impervious boundaries were imposed on both circular faces of each aggregate). If the steady-state approximation is adequate, Eq. (2) can be used to describe the necessary conditions for development of anaerobiosis within these six aggregates. In cases where central regions of aggregates became anaerobic, it was expected that Se(VI) reduction to adsorbable and less soluble Se(IV), and possibly to insoluble Se(0) within these zones would lower the local chemical potential of Se(VI). This, in turn, would initiate diffusion of Se(VI) toward reducing core regions from more aerated outer regions of the aggregates. Thus, the total Se concentration would increase within reducing zones, and become depleted in aerated regions within the same aggregate. After a period of incubation, the synthetic aggregates were scanned with the SXRFM in order to determine the spatial distribution of Se in order to test for the development of such patterns.

Synthetic soil aggregates were prepared using soils collected from the Kesterson National Wildlife Refuge in an area also mapped as Albic Natraqualf. These soils had no prior history of exposure to the seleniferous drain waters, and had a Se concentration of <0.5 mg kg^{-1}. (Contaminated surface soils at Kesterson Reservoir commonly had total Se concentrations >4 mg kg^{-1}.) The original field soil contained U.S.D.A.-size fractions of clay, silt, and sand in 20%, 37%, and 43% portions, respectively. In order to minimize noise in X-ray fluorescence arising from particle-size influences (Bertin 1978), most of the >50 μm fraction of this field sample was removed via sedimentation. (Other experimental evidence from the original soil material showed that Se concentration gradients are easily resolvable, but that smoother spatial maps could be obtained with finer grain-size). The final laboratory soil material contained clay, silt, and sand size fractions in 32%, 60%, and 8% portions, respectively, and 1% organic matter. The laboratory soil aggregates were formed by mixing tap water into homogenized soil material to provide an initial water:soil mass ratio of 0.30 ± 0.04. Laboratory-aggregated soil materials were formed into flat pellets of various sizes, and pressed onto sample holders (Fig. 4). The synthetic soil aggregates ranged in diameter

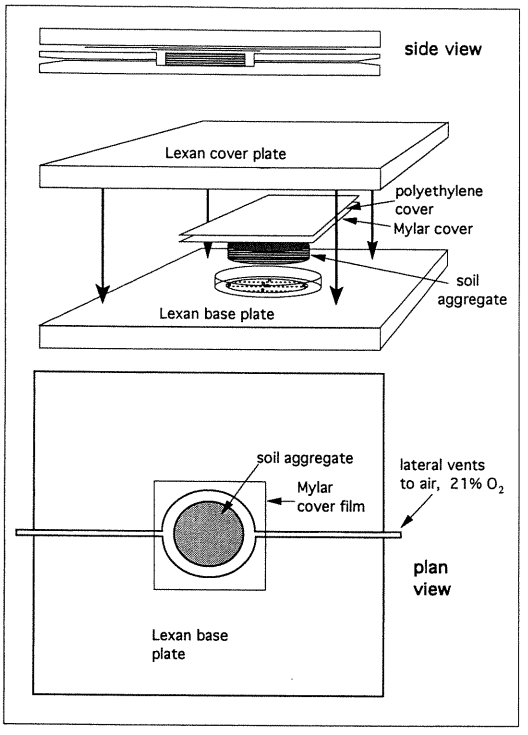

FIG. 4. Synthetic soil aggregate mounting for SXRFM analysis. See text for construction details.

from 10 mm to about 30 mm. Equivalent dry bulk densities of these pellets ranged from 1.1×10^3 kg m^{-3} to 1.2×10^{-3} kg m^{-3}. The square (50-mm sides), 6.35 mm thick, polycarbonate plastic sample holders provided a rigid backing through which gas diffusion was negligible. Aggregates were placed into the central portion of 2.6 ± 0.2 mm deep cavities milled into the plastic. For most samples, large (3 to 10 mm diameter) gaps were provided between the perimeters of the aggregate and borders of the milled cavity. Syringe needles provided lateral ports through which external air equilibrated with the perimeter of the soil aggregates during incubation. In some of the water-saturated samples, the cavity was completely filled with soil.

About 80% of the originally added water was permitted to evaporate from these aggregates over a 2-day period. After this time, selenium was added to each of the samples in an aqueous solution with major ion composition similar to that of agricultural drainage waters. Selenium, was added in this solution at a total concentration of 240 g m^{-3}, primarily (98%) as Se(VI), with the remainder as Se(IV). It should be noted that this concentration is about 10^3 times higher than that of the seleniferous drain waters that contaminated Kesterson Reservoir. The high Se concentration was used to ensure that later microprobe analyses would be able to detect Se distributions with small relative uncertainties. Previous laboratory experiments on these soils indicated that these high Se concentrations did not significantly inhibit microbially mediated Se transformations (Pickering et al. 1994). A preweighed quantity of Se(VI) solution was distributed along the edge of each aggregate via syringe needle, with the source pressure kept within 50 Pa of local atmospheric pressure. The amount of seleniferous water added was varied between individual aggregates in order to obtain saturations ranging from 40 to 100%. This resulted in initial soil Se concentrations ranging from 30 to 70 mg kg^{-1} (mass of Se per wet soil mass). The characteristic soil water sorptivities and Se(VI) diffusivities were large enough relative to the aggregate dimensions to permit practically uniform distributions of water and Se(VI) within several hours. In several aggregates, sections of roots cut from *Scirpus robustus* and *S. californicus*, two common wetland plants, were embedded into the upper surface.

Upon wetting with the seleniferous solution, the open face of the system was sealed with Mylar film (25 μm thickness). The Mylar film was covered with two layers of 70-μm polyethylene film, which in turn was covered with a 3.2-mm-thick polycarbonate plastic top plate. Upon compressing the top plate and intermediate film layers onto the sample and sample holder, the upper surface was also made impervious to gas exchanges. Thus, gas exchange occurred only along the perimeters of aggregates. The various laboratory aggregate samples were incubated for 6 to 17 days, under fluctuating temperatures (27° $\pm$ 5°C). Samples were stored in a humidified container (99 to 100% relative humidity) during the incubation period. Periodic weighing of the samples in their holders indicated no significant changes in water content during the incubation. Periodic extraction of small volumes of gas from the hypodermic needle ports and injection into a polarographic oxygen analyzer (Beckman model 0260, with a custom-built low-volume sensor port) indicated that O_2 concentrations along the aggregate exteriors remained at atmospheric values.

The distributions of Se and several other elements were determined in seven synthetic soil aggregates. Two 10- to 11 mm-diameter aggregates had air-filled porosities (denoted by f_a) of 0.30 and 0.10 (both ± 0.03), respectively. Four 25- to 30-mm diameter soil aggregates were also studied. These four aggregates had f_a values of 0.32, 0.20, 0.10, and 0.07 (all ± 0.04). Sections of *Scirpus* roots were embedded in the 0.10- and 0.20-f_a samples. A final sample (≈30 mm in diameter, f = 0.57 ± 0.04) consisted of a completely water-saturated soil, in which sections of *Scirpus* tissue were embedded. These samples were only scanned with the SXRFM after prescribed incubation periods. Scanning of these samples at their time-zero conditions was not possible because of limited availability of experimental time at the NSLS and because of potential adverse effects on soil microbes. Previous SXRFM experiments on Se(VI) introduced into soil aggregates exhibited essentially homogeneous initial Se distributions.

All SXRFM measurements were performed at the NSLS, beamline X26A. A plan view of the major components within the experimental hutch of the SXRFM was shown in Fig. 2. The collimated incident X-ray beam strikes a sample mounted at a 45° angle. For these experiments, white X-rays emitted from the synchrotron ring were used without a monochrometer. A video monitor was used to position the sample relative to the incident X-ray beam. Fluorescence X-rays were monitored with a Si(Li) energy-dispersive detector (≈200-eV energy resolution at the Se Kα energy) mounted at 90° relative to the incident beam. The Kα energy denotes the photon energy released during L- to K-shell electron transitions. For Se, these photons are in the range of 11.2 keV. Fluorescent X-rays are emitted from all points on the beam path within the sample with approximately exponentially decreasing intensity. Since the incident beam and fluorescence detector are aligned on a common horizontal plane, the measured fluorescence originates from an asymmetric volume within the soil. More specifically, higher spatial resolution is retained along the vertical, and broader horizontal averaging occurs. For this reason, one-dimensional scans of samples were performed along the vertical direction. Scanning of a sample is performed by moving the sample with motorized drives relative to the essentially stationary incident X-ray beam.

For the natural soil aggregates, the SXRFM scans were performed by holding the sample in a fixed position on the beam during a counting interval and moving the sample vertically across the beam path in discrete steps between counting periods. The samples were typically scanned over about 5-mm by 5-mm areas, with vertical and horizontal steps ranging from 50 to 250 μm. The nominally 10-μm beam spot averages over a larger region of the sample because of the substantial thickness. The effective X-ray absorption depth for Se in the soil matrix is about 200 μm; thus, our samples are of effectively infinite thickness.

In the later studies of synthetic aggregates, the sample was scanned slowly while fluorescence data were collected. Using this approach, fluorescence spectra represented moving averages of 0.5-mm vertical traverses. This was done to smooth out small-scale heterogeneities in fluorescence spectra resulting from grain-size effects. For both the natural and synthetic soil aggregates, the background-corrected, beam current-normalized fluorescence count rates were converted into total Se concentrations by equating their average values with independent measurements of bulk concentrations. These latter concentrations were obtained with conventional, energy dispersive X-ray fluorescence spectrometry on the bulk samples (Giauque et al. 1977).

RESULTS AND DISCUSSION

The SXRFM map of total Se concentrations within the field soil aggregate is shown in Fig. 5. The local Se concentration was then taken to be linearly proportional to the background-subtracted Se Kα fluorescence count rate. Note that large variations in total Se concentrations were observed at the scale of about 1 mm. The persistence of high gradients in total Se concentrations suggest that insoluble Se(0) and Se(IV) species account for most of this element. More soluble Se(VI) is expected to uniformly distribute on the aggregate scale via diffusion. Note also that the spatial distribution of Se within this aggregate interior cross-section is neither radial nor apparently random. The sample preparation process could not have introduced more than about 0.3-mm displacements in mineral grain positions, as noted previously. These results indicate that intra-aggregate heterogenei-

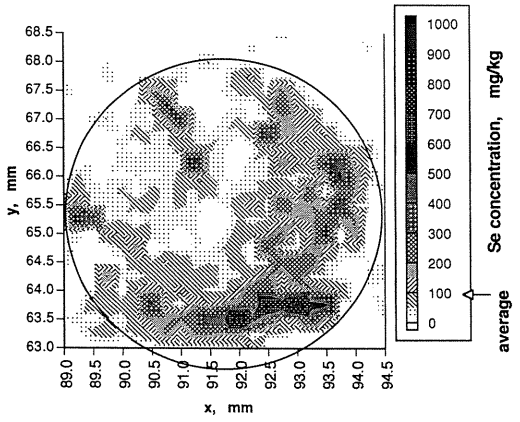

FIG. 5. Spatial distribution of total Se in a natural soil aggregate sampled at Kesterson Reservoir.

ties may be important in initiating reduction in patterns contrary to that of the radially symmetric microsites expected in homogeneous aggregates. Also, within the aggregate, the total Se concentrations are approximated by a lognormal probability distribution as shown in Fig. 6.

Previous experiences with wetting of synthetic soil aggregates with Se(VI) solutions have indicated that uniform short-term Se distributions are easily achieved. The homogeneity with respect to short-term (~1 day) Se distributions is expected based on uniformity of wetting over short distances characteristic of the aggregate scale and previously observed time lags associated with Se reduction. The possibility of Se redistribution in response to localized Se reduction is addressed in the remainder of this study.

The distribution of Se, expressed in terms of normalized Kα fluorescence count rates, along a central transect through the 11-mm-diameter synthetic soil aggregate, is show in Fig. 7. Note that relatively homogeneous distributions of total Se were measured in this sample on day 17. Similar results were obtained in the 10-mm-diameter synthetic soil aggregate, as well as in larger soil aggregates in regions that did not contain embedded plant tissue. Such observations are expected when Se(VI) remains essentially unreduced, and is free to distribute diffusively to minimize concentration gradients. Thus, the presence of reducing zones in these aggregates appears very unlikely. In the context of the two-dimensional (cylindrical) anaerobic microsite model, these observations imply that

$$S \leq \frac{4D_{e,O_2}C_{o,O_2}}{R^2} \tag{7}$$

For these experiments, essentially no deviations from atmospheric concentrations of O_2 were measured at the aggregate exteriors. Therefore the $C_{o,O_2} \approx 270$ g m^{-3} for O_2 at the aggregate exteriors. D_{e,O_2} values may be estimated from various model functions that rely on calculations from f_a. The calculated D_{e,O_2} values will have large uncertainties, partly because of the ± 0.03 absolute uncertainties in the f_a, and also because

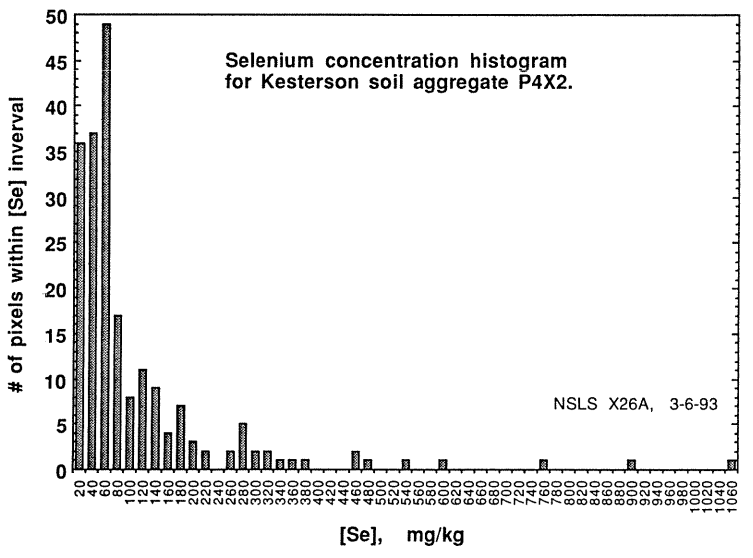

FIG. 6. Histogram of total Se concentrations measured in the Kesterson Reservoir soil aggregate. The distribution function for total Se is approximately log-normal.

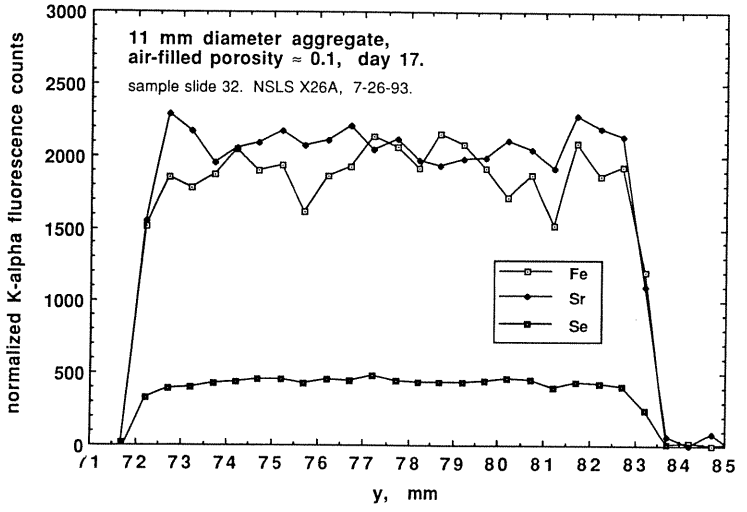

FIG. 7. Spatial distributions of total Se, Fe, and Sr along a central transect through the 11-mm-diameter synthetic soil aggregate after 17 days of incubation. Data are displayed as (background-subtracted) normalized Kα fluorescence count rates.

no single model for porous media diffusivity is sufficiently general to account for influences of pore-structure differences. For our present purpose, we used the regression relation of Sallam et al. (1984),

$$D_{e,O_2} = \frac{f_a^{3.1}}{f^2} D_{o,O_2} \tag{8}$$

where f represents the total porosity, and D_{o,O_2} is the O_2 diffusivity in air, while recognizing that deviations from predicted D_{e,O_2} can be large (e.g., Xu et al., 1992). The D_{o,O_2} values ranged from 2.05×10^{-5} to 2.17×10^{-5} m^2 s^{-1} for the range of temperatures covered during incubation. For the case of $f = 0.57 \pm 0.02$ and $f_a = 0.07 \pm 0.04$, values of D_e from Eq. (8), range from 1.0×10^{-4} to 6.6×10^{-3} m^2 day^{-1}. Using parameters characteristic of the aggregates, along with Eqs. (7) and (8), we may estimate upper limits on O_2 consumption rates. Using the lowest estimated D_e in the largest, wettest aggregates (without added plant tissue), this analysis indicates that $S < 500$ g O_2 m^{-3} day^{-1}. This upper limit on S is still much higher than values typically reported for bulk soil respiration rates. For example, soil respiration rates from Black (1968), Smith (1980), and Buyanovsky et al. (1986) are in the range of 20 to 80 g O_2 m^{-3} day^{-1}. Estimates of S, based upon simplified models used to obtain Eqs. (2) and (7) can be difficult to apply because of the need for approximately steady-state conditions and uncertainties in values of D_e. Direct measurements of S on individual aggregates would have provided a better understanding of these systems. An example of a such an experimental design is provided in Leffelaar (1986 and 1993).

Also shown in Fig. 7 are normalized fluorescence count rate transects for total Fe and total Sr in the aggregate. Note that these elements are also distributed relatively uniformly and that the boundaries of the aggregate are easily recognized from the drop-offs in count rates of each of the constituents.

The total Se concentration along an aggregate transect which intercepted an embedded *Scirpus* root section is shown in Fig. 8. The SXRFM mapping was performed after 17 days of incubation. (Measurements on the initial Se distribution in this sample were not possible because of scheduling conflicts. However, results of SXRFM mapping on very similar samples at and near time zero displayed essentially homogeneous Se profiles similar to those shown in Fig. 7). The *Scirpus* root-embedded aggregate had an $f_a = 0.10 \pm 0.03$. The location of the root section was determined directly from the Fe and Sr concentration profiles also obtained in the X-ray fluorescence spectra. The root position is clearly indicated by local minima in both Fe and Sr count rates. Note that only in regions adjacent to the decomposing root section is there evidence of Se accumulation, indicating that this region experienced reducing conditions during the incubation period. The relatively uniform concentrations of Se throughout the rest of the aggregate indicate that oxidizing conditions prevailed in all other areas of the aggregate. Al-

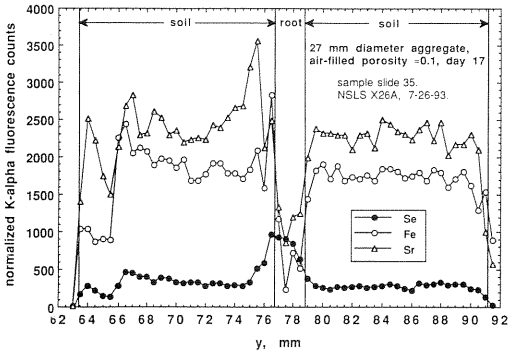

FIG. 8. Spatial distributions of total Se, Fe, and Sr along a transect through a decomposing *Scirpus* root, laterally-embedded within a 27-mm-diameter synthetic soil aggregate after 17 days of incubation. Data are displayed as (background-subtracted) normalized Kα fluorescence count rates.

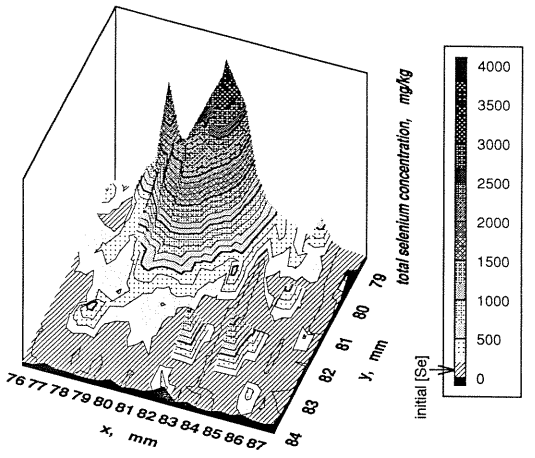

FIG. 9. Two-dimensional SXRFM map of total Se concentration in the vicinity of the *Scirpus* root embedded in water-saturated soil after 7 days of incubation.

though redox-induced transport of Fe may be possible, this element was highly correlated with Sr (which is largely associated with the solid phase and will not undergo redox transformations) in this and all other samples tested. Such correlations indicate that mobilization of Fe(II) did not occur to any significant extent during the course of these experiments.

Both one-dimensional transects and two-dimensional maps of total Se were generated on days 6 and 7 for the case of a *Scirpus* root cross section embedded within a water-saturated sediment ($f = 0.57$, $f_a = 0$). (Again, measurements on the initial Se distribution in this sample were not possible because of scheduling conflicts.) The root-sediment boundary was determined from Fe and Sr concentration profiles. The 2-dimensional distribution of total Se concentrations in this case is shown in Fig. 9. (The coordinates in this figure are those of the x-y stage on the SXRFM.) Note that very large accumulations of Se were observed within the 7-day incubation period. More than 20-fold increases in total Se were measured in sediments near the root interface. Although the distributions shown through the data in Fig. 9 are for total Se, the evolution of the profile is hypothesized to result from reduction of Se(VI).

A qualitative set of radial distributions for Se(VI), Se(IV), and Se(0), which may be associated with the total Se distribution (Fig. 9), is presented in Fig. 10. The region in which total Se concentrations were measurably enriched must correspond to a zone dominated by essentially immobile species. Otherwise, the very steep concentration gradients would result in diffusive dissipation of the accumulated Se. Thus, Se(0), and possibly Se(IV), accumulated in this zone because these are the much less mobile species. The presence of these species indicates Se reduction. The Se(VI) concentration is expected to approach zero in this region of total Se accumulation since this species is very unstable under reducing conditions. At each position, the sums of Se(0), Se(IV), and

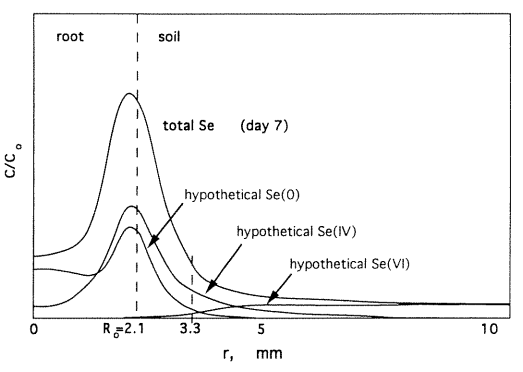

FIG. 10. Hypothetical radial distributions of Se(VI), Se(IV), and Se(0) after 7 days of incubation in the vicinity of the decomposing *Scirpus* root embedded in sediment.

Se(VI) concentrations are constrained to add up to the total Se concentration.

Although the details of the Se(VI), Se(IV), and Se(0) concentration distributions remain unknown, the simplified model based on Eq. (3) may be used to determine whether or not Se(VI) diffusion to a reducing zone could account for the magnitude of the observed total Se accumulation. This calculation was performed by setting the radius of the Se(VI) zero-concentration boundary at $R^* = 3.3$ mm (Fig. 3), based on the mean radius at which the total Se concentration was elevated to twice the initial concentration. For this model, $D_{e,Se(VI)}$ was approximated by values calculated as 35 $mm^2\ d^{-1}$ using Eq. (6), assuming a reasonable value of $\alpha = 0.65$. This estimated value of $D_{e,Se(VI)}$ is in very good agreement with temperature-corrected values of D_{e,SO_4} reviewed by Iversen and Jorgensen (1993) for sediments having the same porosity. The time-dependence of the Se(VI) diffusion rate into the reducing zone at 3.3 mm was calculated from Eq. (3). This result was then integrated with respect to time to obtain the modeled cumulative diffusive flux. The modeled cumulative diffusive flux of Se into the reducing zone is shown in Fig. 11, along with the case in which $D_{e,Se(VI)}$ is half as large as the predicted magnitude. The measured average total Se concentration within the reducing zone on days 6 and 7 are plotted in Fig. 11 for comparison. Discrepancies between measured and modeled results probably originate from uncertainties in (i) the spatial and temporal distribution of reduction activity, (ii) the actual concentrations of Se(VI) in the reducing region, (iii) $D_{e,Se(VI)}$, and (iv) likely counter-diffusion of Se(IV). In view of these uncertainties, diffusive transport of Se(VI) to a reducing zone appears to adequately account for the accumulation of Se.

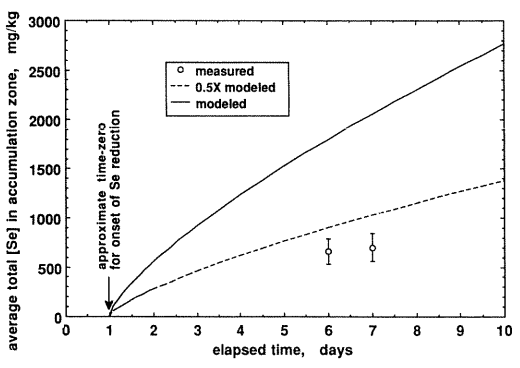

FIG. 11. Model calculations of time-dependence of the average total Se concentration in reducing zone around the decomposing *Scirpus* root, assuming radial diffusion to a zero concentration boundary at r = 3.3 mm. The (day 6 and 7) SXRFM-measured average values of total Se concentration in this zone are also shown. The lower curve represents predictions based on an effective Se(VI) diffusivity which is one-half that of the estimated $D_{e,Se(VI)}$ (upper curve).

CONCLUSION

Synchrotron X-ray fluorescence microprobe analyses of Se-contaminated soil aggregates obtained from Kesterson Reservoir indicated the presence of localized zones, typically with dimensions of ≈1 mm, in which significantly elevated concentrations of total Se occur. Such small-scale heterogeneities in Se concentrations can only persist when effective diffusivities of the dominant Se species are very low. Both Se(0) and various possible solid phase forms of Se(IV) may account for these localized Se-concentrated zones. If reoxidation of Se(0) and Se(IV) in soils occurs primarily as reactions at solid phase surfaces, highly localized accumulations of reduced species may influence these reaction rates. Reoxidation of Se(0) and Se(IV) in microsites may occur slowly relative to the case where these species are uniformly dispersed throughout aggregates. In the former case, reoxidation may proceed by sequentially oxidizing layers of Se from a limited area. In the latter case, all reduced Se species may be simultaneously exposed to oxidants. Thus, localization of reduced Se species may partially explain the slow reoxidation rates observed for Se in Kesterson Reservoir soils (Tokunaga et al. 1991).

The present study of Se distributions in both natural and laboratory-constructed soil aggregates provides examples of how trace elements with redox-dependent solubilities can be used to study variable redox environments in soils. The application of the SXRFM for trace element mapping within soil aggregates illustrates the potential usefulness of this tool in soil science. It is emphasized in this context that much higher spatial resolution (approaching 1 μm) is possible with this method and that the ≈100-μm resolution associated with the present study was due to sample thickness effects.

The laboratory experiments demonstrated the potential importance of decomposing organic matter in generating localized reducing zones for Se accumulation. However, the simple model of Se(VI) diffusion to a cylindrical sink overestimated the measured amount of Se accumulation in the vicinity of a section of *Scirpus* root embedded in a water-saturated sediment. Improved understanding of the dynamics of such processes, hence, improved modeling, awaits experiments in which maps of individual Se species are obtained along with high-resolution measurements of spatial distributions of diffusivities and respiration rates.

Improved resolution with respect to chemical speciation in SXRFM is another current area of expanding research. Most SXRFM studies to date have provided maps of total elemental concentrations within samples. As our previous discussions indicated, direct mapping of individual oxidation states, i.e., Se(VI), Se(IV), and Se(0) mapping, is needed to better understand the complex dynamics of reactions and transport. Synchrotron-based X-ray absorption spectroscopy (XAS) permits direct determinations of valence in elements that undergo oxidation and reduction (Waychunas et al. 1983; Wong et al. 1984; Waychunas 1987; Brown and Parks 1989). Shifts in the position of the X-ray absorption edge, typically by about 2 to 4 eV per oxidation state, may be used to directly determine the valence composition of elements of interest. This feature of XAS has recently been utilized in research conducted at the Stanford Synchrotron Radiation Laboratory (I.J. Pickering et al. 1994) to demonstrate the occurrence of Se(0) in Kesterson Reservoir soils and to track the reduction of Se(VI) to Se(IV), and ultimately to Se(0), in laboratory experiments. By inclusion of a monochrometer in the SXRFM, with which characteristic features of the Se X-ray absorption edge are obtained for each pixel, one could obtain individual maps for Se(VI), Se(IV), and Se(0) concentrations. Such micro-XAS studies with Se in sediments will be initiated in the near future. Recent examples of the value of this approach include studies of Cr by Sutton et al. (1993) and by Bajt et al. (1993), and U by Bertsch et al. (1994). Synchrotron-based X-ray methods have tremendous future applications in studies of soils. The capabilities of direct, nondestructive measurements with respect to elemental mapping, speciation, and elucidation of bonding structures of a wide range of elements make these methods highly attractive research tools.

ACKNOWLEDGMENTS

This work was carried out under U.S. Department of Energy Contracts No. DE-AC03-76SF00098, DE-FG02-92BR14244 (SRS), and DE-AC02-76CH00016 (Brookhaven National Laboratory). Research was, in part, carried out at the National Synchrotron Light Source (NSLS), Brookhaven National Laboratory, which is supported by the U.S. Department of Energy, Division of Materials Sciences and Division of Chemical Sciences. We also thank Mark L. Rivers (Center for Advanced Radiation Sources, The University of Chicago), and the staff at NSLS. T.K. Tokunaga gratefully acknowledges funding provided through the Laboratory Directed Research and Development program of Lawrence Berkeley Laboratory and support of the research proposal by Sally Benson and Tom McEvilly. We thank Steve Flexser and Jiamin Wan of Lawrence Berkeley Laboratory for helpful comments on the preliminary manuscript. We also thank the anonymous reviewers for their very helpful suggestions.

REFERENCES

Anderson, M. S., H. W. Lakin, K. C. Beeson, F. F. Smith, and E. Thacker. 1961. Selenium in agriculture. Agricultural Handbook No. 200. Agric. Res. Service, U.S. Dept. Agric. Government Printing Office, Washington, DC.

Bajt, S., S. B. Clark, S. R. Sutton, M. L. Rivers, and J. V. Smith. 1993. Synchrotron X-ray microprobe determination of chromate content using X-ray absorption near-edge structure. Anal. Chem. 65:1800–1804.

Benson, S. M., A. F. White, S. Halfman, S. Flexser, and M. Alavi. 1991. Groundwater contamination at Kesterson Reservoir, California 1. Hydrogeologic setting and conservative solute transport. Water Resour. Res. 27:1071–1084.

Bertin, E. P. 1978. Introduction to X-ray spectrometric analysis. Plenum Press, New York.

Bertsch, P. M., D. B. Hunter, S. R. Sutton, S. Bajt, and M. L. Rivers. 1994. In-situ chemical speciation of uranium in soils and sediments by micro X-ray absorption spectroscopy. Envir. Sci. Tech. 28:980–984.

Black, C. A. 1968. Soil-Plant Relationships. 2nd Ed. J. Wiley & Sons, Inc., New York.

Brown, G. E. Jr., and G. A. Parks. 1989. Synchrotron-based X ray absorption studies of cation environ-

ments in earth materials. Rev. Geophys. 27:519–533.

Buyanovsky, G. A., G. H. Wagner, and C. J. Gantzer. 1986. Soil respiration in a winter wheat ecosystem. Soil Sci. Soc. Am. J. 50:338–344.

Currie, J. A. 1961. Gaseous diffusion in the aeration of aggregated soils. Soil Sci. 92:40–45.

Currie, J. A. 1965. Diffusion within soil microstructure. A structural parameter for soils. J. Soil Sci. 16:279–289.

Elrashidi, M. A., D. C. Adriano, S. M. Workman, and W. L. Lindsay. 1987. Chemical equilibrium of selenium in soils: A theoretical development. Soil Sci. 144:141–152.

Freney, J. R., O. T. Denmead, and J. R. Simpson. 1979. Nitrous oxide emission from soils at low moisture contents. Soil Biol. Biochem. 11:167–173.

Geering, H. R., E. E. Cary, L. H. P. Jones, and W. H. Allaway. 1968. Solubility and redox criteria for the possible form of selenium in soils. Soil Sci. Soc. Am. Proc. 32:35–40.

Giauque, R. D., R. B. Garrett, and L. Y. Goda. 1977. Determination of forty elements in geochemical samples and coal fly ash by X-ray fluorescence spectrometry. Anal. Chem. 49:1012–1017.

Hillel, D. 1980. Fundamentals of soil physics. Academic Press, New York.

Iversen, N., and B. B. Jorgensen. 1993. Diffusion coefficients of sulfate and methane in marine sediments: Influence of porosity. Geochim. Cosmochim. Acta 57:571–578.

Jacob, C. E., and S. W. Lohman. 1952. Nonsteady flow to a well of constant drawdown in an extensive aquifer. Trans. Am. Geophys. Union 33:559–569.

Jones, K. W., and B. M. Gordon. 1989. Trace element determinations with synchrotron-induced X-ray emission. Anal. Chem. 61:341A-358A.

Leffelaar, P. A. 1986. Dynamics of partial anaerobiosis, denitrification, and water in a soil aggregate: Experimental. Soil Sci. 142:352–366.

Leffelaar, P. A. 1993. Water movement, oxygen supply and biological processes on the aggregate scale. Geoderma 57:143–165.

Long, R. H. B., S. M. Benson, T. K. Tokunaga, and A. Yee. 1990. Selenium immobilization in a pond sediment at Kesterson Reservoir. J. Environ. Qual. 19:302–311.

Nazar, P. G. 1990. Soil survey of Merced County, California, Western part. U.S. Dept. Agric., Soil Conservation Service. U.S. Government Printing Office, Washington, DC.

Neal, R. H., G. Sposito, K. M. Holtzclaw, and S. J. Traina. 1987. Selenite adsorption on alluvial soils: I. Soil composition and pH effects. Soil Sci. Soc. Am. J. 51:1161–1165.

Ohlendorf, H. M. 1989. Bioaccumumation and effects of selenium in wildlife. In Selenium in Agriculture and the Environment, Soil Sci. Soc. Am. Special Pub. 23.

Parkin, T. B. 1987. Soil microsites as a source of denitrification variability. Soil Sci. Soc. Am. J. 51:1194–1199.

Pickering, I. J., G. E. Brown, Jr., and T. K. Tokunaga. 1994. X-ray absorption spectroscopy of selenium-contaminated soils. Stanford Synchrotron Radiation Laboratory 1993 Activity Report. Stanford University, Stanford, CA.

Rivers, M. L., S. R. Sutton, K. W. Jones. 1991. Synchrotron X-ray fluorescence microscopy. Synchrotron Radiation News 4:23–26.

Robinson, R. A., and R. H. Stokes. 1959. Electrolytic solutions. Butterworths, London.

Rosenfeld, I., and O. A. Beath. 1964. Selenium geobotany, biochemistry, toxicity, and nutrition. Academic Press, New York.

Sallam, A., W. A. Jury, and J. Letey. 1984. Measurement of gas diffusion coefficient under relatively low air-filled porosity. Soil Sci. Soc. Am. J. 37:189–193.

Sharma, S., and R. Singh. 1983. Selenium in soil, plant, and animal systems. CRC Crit. Rev. Environ. Control 13:23–50.

Smith, K. A. 1977. Soil aeration. Soil Sci. 123:284–291.

Smith, K. A. 1980. A model of the extent of anaerobic zones in aggregated soils and its potential application to estimates of denitrification. J. Soil Sci. 31:263–277.

Smith, L. P. 1937. Heat flow in an infinite solid bounded internally by a cylinder. J. Appl. Physiol. 8:441–448.

Sutton, S. R., K. W. Jones, B. Gordon, M. L. Rivers, S. Bajt, and J. V. Smith. 1993. Reduced chromium in olivine grains from lunar basalt 15555: X-ray absorption near edge structure (XANES). Geochim. Cosmochim. Acta 57:461–468.

Sutton, S. R., M. L. Rivers, S. Bajt, and K. W. Jones. 1993. Synchrotron X-ray fluorescence microprobe analysis with bend magnets and insertion devices. Nucl. Inst. Meth. B75:553–558.

Tokunaga, T. K., D. S. Lipton, S. M. Benson, A. W. Yee, J. O. Oldfather, E. C. Duckart, P. W. Johannis, and K. E. Halvorsen. 1991. Soil selenium fractionation, depth profiles and time trends in a vegetated upland at Kesterson Reservoir. Water Air Soil Pollut. 57/58:31–41.

Waychunas, G. A., J. Apted, and G. E. Brown, Jr. 1983. X-ray K-edge absorption spectra of Fe minerals in model compounds: near edge structure. Phys. Chem. Minerals 10:1–9.

Waychunas, G. A. 1987. Synchrotron radiation XANES spectroscopy of Ti in minerals: Effects of Ti bonding distances, Ti valence, and site geometry on absorption edge structure. Am. Mineralogist 72:89–101.

Weres, O., A. R. Jaouni, L. Tsao. 1989. The distribution, speciation and geochemical cycling of selenium in a sedimentary environment, Kesterson Reservoir, California, U.S.A. Appl. Geochem. 4:543–563.

White, A. F., S. M. Benson, A. W. Yee, H. A. Wollenberg, and S. Flexser. 1991. Groundwater contamination at the Kesterson Reservoir, California 2. Geochemical parameters influencing selenium mobility. Water Resour. Res. 27:1085–1098.

Wong, J., F. W. Lytle, R. P. Messmer, and D. H.

Maylotte. 1984. K-edge absorption spectra of selected vanadium compounds. Phys. Rev. B Condens. Matter 30:5596–5610.

Wu, Y., A. C. Thompson, J. H. Underwood, R. D. Giauque, K. Chapman, M. L. Rivers, and K. W. Jones. 1990. A tunable X-ray microprobe using synchrotron radiation. Nucl. Instrum. Methods Phys. Res. A291:146–151.

Xu, X., J. L. Nieber, and S. C. Gupta. 1992. Compaction effect on the gas diffusion coefficient in soils. Soil Sci. Soc. Am. J. 56:1743–1750.

Zawislanski, P. T., T. K. Tokunaga, S. M. Benson, J. O. Oldfather, and T. N. Narasimhan. 1992. Bare soil evaporation and solute movement in selenium-contaminated soils of Kesterson Reservoir, CA. J. Environ. Qual. 21:447–457.